

## Two-dimensional elastic turbulence

S. Berti,<sup>1,2</sup> A. Bistagnino,<sup>3</sup> G. Boffetta,<sup>3,4</sup> A. Celani,<sup>5</sup> and S. Musacchio<sup>3</sup>

<sup>1</sup>*Department of Mathematics and Statistics, University of Helsinki, P.O. Box 68, FIN-00014 Helsinki, Finland*

<sup>2</sup>*Laboratoire de Spectrométrie Physique CNRS, Boîte Postale 87, 38402 Saint Martin d'Hères, France*

<sup>3</sup>*Dipartimento di Fisica Generale, INFN and CNISM, Via Pietro Giuria 1, 10125, Torino, Italy*

<sup>4</sup>*CNLS, Los Alamos National Laboratory, Los Alamos, New Mexico 87545, USA*

<sup>5</sup>*CNRS URA 2171, Institut Pasteur, 75724 Paris Cedex 15, France*

(Received 31 October 2007; published 29 May 2008)

We report numerical evidence of elastic turbulence phenomenology in a two-dimensional periodic Kolmogorov flow. By direct numerical simulations of the Oldroyd-B viscoelastic model at very small Reynolds numbers, we find that above the elastic instability threshold the flow develops an elastic turbulent regime. We observe that both the turbulent drag and the Lyapunov exponent increase with the Weissenberg number, indicating the presence of a disordered, turbulentlike mixing flow. The energy spectrum develops a power-law scaling range with an exponent close to the experimental and theoretical expectations.

DOI: 10.1103/PhysRevE.77.055306

PACS number(s): 47.27.-i, 47.27.E-

One of the most remarkable effects of highly viscous polymer solutions that has been recently observed in experiments is the development of an “elastic turbulence” regime in the limit of strong elasticity [1]. The flow of polymer solution in this regime displays irregularities typical of turbulent flows (broad range of active scales and growth of flow resistance) even at low velocity and high viscosity, i.e., in the limit of vanishing Reynolds number. As a consequence of turbulent motion at small scales, elastic turbulence has been proposed as an efficient technique for mixing in very low Reynolds flows, such as in microchannel flows [2–4]. Despite its great technological interest, elastic turbulence is still only partially understood from a theoretical point of view. Recent theoretical predictions are based on simplified versions of viscoelastic models and on the analogy with magnetohydrodynamics (MHD) equations [5,6].

In this Rapid Communication, we investigate the phenomenology of elastic turbulence in direct numerical simulation of polymer solutions in two-dimensional Kolmogorov shear flow. Our main objective is to show that usual viscoelastic models and very simplified geometry without boundaries are able to capture, in the limit of vanishing Reynolds numbers, the main phenomenology of elastic turbulence, i.e., irregular temporal behavior and spatially disordered flow. Despite the important geometrical differences, our numerical results are in remarkable agreement with experimental observations of elastic turbulence: this suggests the possibility of understanding elastic turbulence on the basis of known viscoelastic models.

To describe the dynamics of dilute polymer solutions, we adopt the well known linear Oldroyd-B model [7],

$$\partial_t \mathbf{u} + (\mathbf{u} \cdot \nabla) \mathbf{u} = -\nabla p + \nu \Delta \mathbf{u} + \frac{2\eta\nu}{\tau} \nabla \cdot \boldsymbol{\sigma} + \mathbf{f}, \quad (1)$$

$$\partial_t \boldsymbol{\sigma} + (\mathbf{u} \cdot \nabla) \boldsymbol{\sigma} = (\nabla \mathbf{u})^T \cdot \boldsymbol{\sigma} + \boldsymbol{\sigma} \cdot (\nabla \mathbf{u}) - 2 \frac{(\boldsymbol{\sigma} - \mathbf{I})}{\tau}, \quad (2)$$

where  $\mathbf{u}$  is the incompressible velocity field and the symmetric positive definite matrix  $\boldsymbol{\sigma}$  represents the normalized con-

formation tensor of polymer molecules, and  $\mathbf{I}$  is the unit tensor. The solvent viscosity is denoted by  $\nu$ , and  $\eta$  is the zero-shear contribution of polymers to the total solution viscosity  $\nu_r = \nu(1 + \eta)$  and is proportional to the polymer concentration. In the absence of flow,  $\mathbf{u} = \mathbf{0}$ , polymers relax to the equilibrium configuration and  $\boldsymbol{\sigma} = \mathbf{I}$ . The trace  $\text{tr } \boldsymbol{\sigma}$  is therefore a measure of polymer elongation.

The simplest geometrical setup that will prove useful to study the elastic turbulence regime for viscoelastic flows is the periodic Kolmogorov flow in two dimensions [8]. With the forcing  $\mathbf{f} = (F \cos(y/L), 0)$ , the system of equations (1) and (2) has a laminar Kolmogorov fixed point given by

$$\mathbf{u} = (U_0 \cos(y/L), 0),$$

$$\boldsymbol{\sigma} = \begin{pmatrix} 1 + \tau^2 \frac{U_0^2}{2L^2} \sin^2(y/L) & -\tau \frac{U_0}{2L} \sin(y/L) \\ -\tau \frac{U_0}{2L} \sin(y/L) & 1 \end{pmatrix} \quad (3)$$

with  $F = [\nu U_0(1 + \eta)]/L^2$  [9]. The laminar flow fixes a characteristic scale  $L$ , velocity  $U_0$ , and time  $T = L/U_0$ . In terms of these variables, we define the Reynolds number as  $\text{Re} = \frac{U_0 L}{\nu_r}$  and the Weissenberg number as  $\text{Wi} = \frac{\tau U_0}{L}$ . The ratio of these numbers defines the elasticity of the flow  $\text{El} = \text{Wi}/\text{Re}$ .

It is well known that the Kolmogorov flow displays instability with respect to large-scale perturbations, i.e., with wavelength much larger than  $L$ . In the Newtonian case, the instability arises at  $\text{Re}_c = \sqrt{2}$  [10]. At small Reynolds numbers, the presence of polymers can change the stability diagram of laminar flows [11,12] or can induce elastic instabilities that are not present in Newtonian fluids [9,13–15], even in the case of periodic flows [16]. In this respect, the Kolmogorov flow is no exception, and recent analytical and numerical investigations have offered the complete instability diagram in the  $\text{Re}$ - $\text{Wi}$  plane [9]. For the purpose of the present work, we just have to recall that linear stability analysis shows that for sufficiently large values of elasticity, the Kolmogorov flow displays purely elastic instabilities,

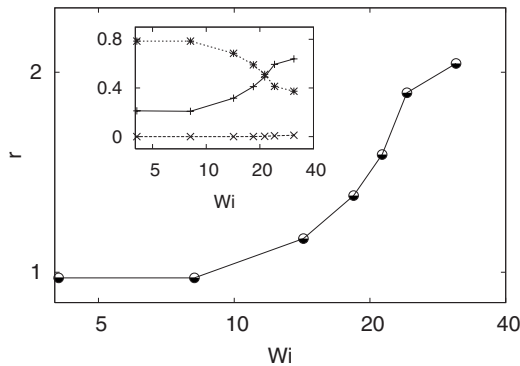


FIG. 1. Mean power injection normalized with its laminar value  $r = P/P_{\text{lam}}$  as a function of  $Wi = \tau U/L$  for a set of simulations with  $\nu = 0.769$ ,  $\eta = 0.3$ ,  $L = 1/4$ , and  $\tau = 4$ . The elasticity is  $El = 64$  and the maximum Reynolds number  $Re = Wi/El$  is  $Re = 0.48$ . Inset: amplitude of the Reynolds stress  $\Pi_r$  ( $\times$ ), polymer stress  $\Pi_p$  ( $+$ ), and viscous stress  $\Pi_v$  ( $*$ ) nondimensionalized by the total stress amplitude  $FL$ .

even at vanishing Reynolds number (see Fig. 1 of [9]). We remark that the fact that the basic flow has rectilinear streamlines does not exclude the onset of the elastic instability [17]. Above the elastic instability, the flow can develop a disordered secondary flow that persists in the limit of vanishing Reynolds number and eventually leads to the elastic turbulence regime [18].

The equations of motion (1) and (2) are integrated by means of a pseudospectral method implemented on a two-dimensional grid of size  $L_0 = 2\pi$  with periodic boundary conditions at resolution up to  $1024^2$ . Numerical integrations of viscoelastic models are limited by Hadamard instabilities associated with the loss of positiveness of the conformation tensor [19]. These instabilities are particularly important at high elasticity and limit the possibility of investigating the elastic turbulent regime by direct implementation of equations (1) and (2). To overcome this problem, we have implemented an algorithm based on a Cholesky decomposition of the conformation matrix that ensures symmetry and positive definiteness [20]. While this allows us to safely reach high elasticity, it has a cost in terms of limited resolution and large computing time.

One of the main features of the transition to a turbulent regime is the growth of the flow resistance to external forcing. This can be quantified as the power needed to maintain a given mean velocity in the turbulent flow. The power injection in Eq. (1) is  $P = \langle \mathbf{f} \cdot \mathbf{u} \rangle$ , which, for the laminar flow (3), becomes  $P_{\text{lam}} = U_0^2 \nu (1 + \eta) / (2L^2)$ . A remarkable feature of the Kolmogorov flow is that even in the turbulent regime, the mean velocity and conformation tensor are accurately described by sinusoidal profiles [21]:  $\langle u_x \rangle = U \cos(y/L)$ ,  $\langle \sigma_{xy} \rangle = -\Sigma \sin(y/L)$  with different amplitudes with respect to the laminar fixed point. Therefore, the reduced average power injection for the turbulent flow is simply

$$r = \frac{P}{P_{\text{lam}}} = \frac{FL^2}{\nu(1 + \eta)U}. \quad (4)$$

Figure 1 shows the behavior of the power injection as a

function of the Weissenberg number  $Wi = \tau U/L$ , which shows a transition to a turbulentlike regime for  $Wi > 15$ .

Because the Reynolds number in Fig. 1 is always small, and therefore the inertial term in Eq. (1) is negligible, it is natural to ask which is the source of turbulent fluctuations. The momentum budget, in stationary conditions, reads

$$\partial_y \Pi_r = \partial_y (\Pi_v + \Pi_p) + f_x, \quad (5)$$

where  $\Pi_r = \langle u_x u_y \rangle$  is the usual Reynolds stress,  $\Pi_v = \nu \partial_y \langle u_x \rangle$  is the viscous stress, and  $\Pi_p = 2\nu\eta\tau^{-1} \langle \sigma_{xy} \rangle$  is the stress induced by polymers. The numerical observation that also the Reynolds stress is well described by a monochromatic profile,  $\langle u_x u_y \rangle = U_2 \sin(y/L)$ , allows us to write the momentum budget for the amplitudes as  $FL = U_2 + \nu U/L + (2\nu\eta/\tau)\Sigma$ . The inset of Fig. 1 shows the different contributions (normalized with the total stress) as a function of  $Wi$ . In the laminar regime ( $Wi \rightarrow 0$ ),  $U_2 = 0$ , and from Eq. (3) one has  $\Pi_p/\Pi_v = \eta$ . Above the transition to elastic turbulence, the polymer stress starts growing and reaches a value larger than viscous stress at the maximum Weissenberg number. The contribution of the Reynolds stress always remains smaller than  $10^{-2}$ , confirming the irrelevance of inertial terms. This is the hallmark of elastic turbulence where elastic stress has the role played by the Reynolds stress in purely hydrodynamic turbulence.

In order to get more insight into the elastic turbulence flow, in Fig. 2 we show two snapshots of the two-dimensional vorticity field at two different  $Wi$ . The first snapshot is taken at  $Wi = 21.3$ , slightly above the elastic instability threshold. The flow in this regime is still not turbulent and a secondary flow in the form of thin filaments is clearly observable. These small-scale filaments, moving along the  $x$  direction, are elastic waves, reminiscent of the Alfvén waves propagating in the presence of a large-scale magnetic field in plasma. Indeed, the possibility of observing elastic waves in polymer solution was theoretically predicted within a simplified uniaxial elastic model [6] that has strong formal analogies with MHD equations, but they were never observed before.

At higher values of elasticity, the vorticity pattern becomes progressively more irregular with chaotic motion of filaments. At  $Wi = 31$ , we observe a highly irregular pattern in which the underlying basic flow is hardly distinguishable. This is the regime of elastic turbulence in which the flow develops active modes at all the scales. Figure 3 shows the power spectrum of velocity fluctuations averaged over several configurations such as the one shown in Fig. 2. A power-law behavior  $E(k) \simeq k^{-\alpha}$  is clearly observable with a spectral exponent  $\alpha$  larger than 3. Again, this is in agreement with what was observed in laboratory experiments [1,22] and with the theoretical predictions based on the uniaxial model [6].

One of the most promising applications of elastic turbulence is efficient mixing at very low Reynolds number. This is an issue of paramount importance in many industrial problems, namely in microfluidic applications. Indeed, laboratory experiments in curvilinear channels have demonstrated that very viscous polymer solutions in the elastic turbulence regime are very efficient for small-scale mixing [2]. Mixing efficiency of polymer solutions has been studied in various

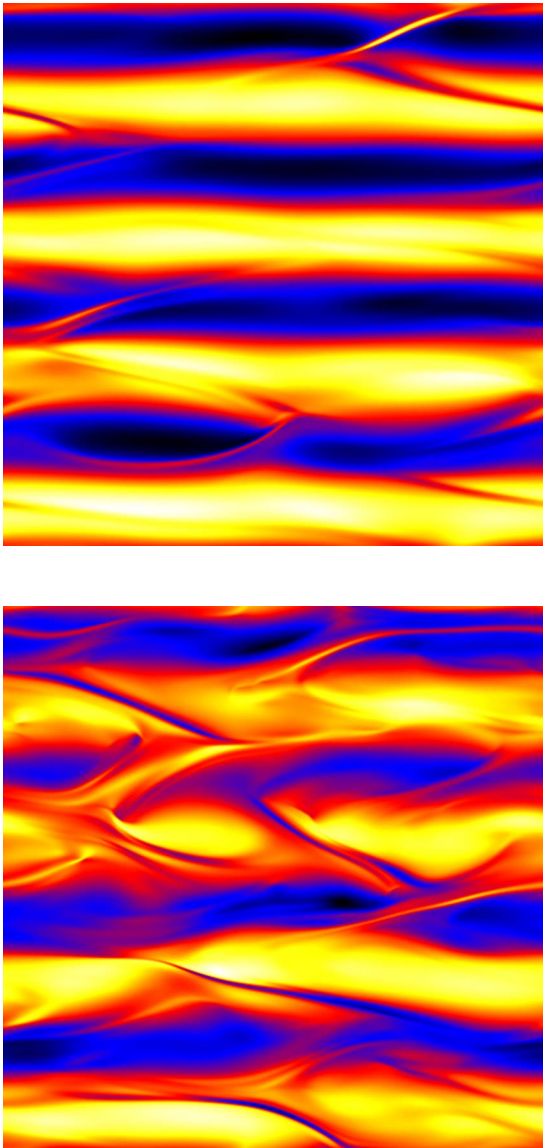


FIG. 2. (Color online) Snapshot of vorticity field at  $Wi=21.3$  (top) and  $Wi=31$  (bottom). The flow is forced with a Kolmogorov forcing  $f_x = F \cos(y/L)$  with  $L = \frac{1}{4}$ . Black (white) corresponds to negative (positive) vorticity.

setups, including microchannels [3] and two-dimensional magnetically driven flows [4]. Because in the elastic turbulent regime the flow is smooth (i.e., the energy spectrum is steeper than  $k^{-3}$ ), a suitable characterization of mixing is given in terms of Lagrangian Lyapunov exponent  $\lambda$  [23]. This is defined as the mean rate of separation of two infinitesimally close particles transported by the flow and, in the present case, is related to the polymer stretching rate [24].

Figure 4 shows the behavior of the Lyapunov exponent rescaled with the polymer relaxation time  $\tau=4$  as a function of  $Wi$ . We observe that, above the transition at  $Wi \approx 10$ ,  $\lambda$  grows and reaches a values  $\approx 1/\tau$  for  $Wi > 31$ . Again, this result is comparable with experimental results in a swirling flow [25], but here mixing is even more efficient as the Lyapunov exponent at given  $Wi$  is larger than in the experiment.

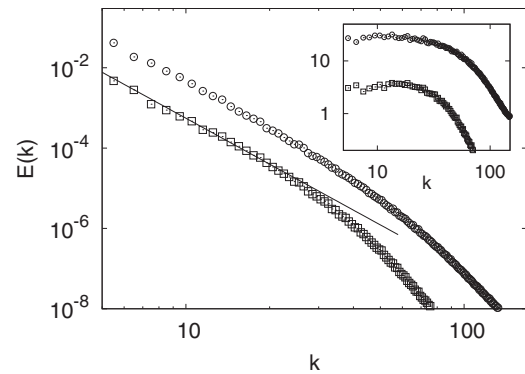


FIG. 3. Velocity fluctuation spectra at  $Wi=21.3$  (squares) and  $Wi=31$  (circles). The line represents the power-law behavior  $k^{-3.8}$ . In the inset, the compensated spectra are shown.

In the inset of Fig. 4, we plot the Cramer function  $G(\gamma)$ , which is defined from the probability density functions of finite-time Lyapunov exponents  $P_t(\gamma) \sim \exp[-tG(\gamma)]$  [23]. As is evident, by increasing  $Wi$ , not only does the degree of mean chaoticity increase, but also the fluctuations become larger. In particular, the distribution of  $\gamma$  becomes asymmetric with a larger relative probability of positive fluctuations. It is remarkable that the same qualitative behavior is observed in the case of high-Reynolds Newtonian turbulence, where the distribution of Lyapunov fluctuations becomes more asymmetric with increasing  $Re$ . This suggests that in elastic turbulence, elasticity (i.e.,  $Wi$ ) plays a similar role to nonlinearity (i.e.,  $Re$ ) in ordinary hydrodynamic turbulence.

Finally, we have investigated the dependence of polymer statistics on the Weissenberg number. In Fig. 5, we show the average squared polymer elongation  $\langle \text{tr } \sigma \rangle$  integrated over the flow volume and the amplitude of cross stress  $\Sigma$ . At small  $Wi$ , these follow the laminar behavior, i.e.,  $2 + Wi^2/4$  and  $Wi/2$ , respectively. At the onset of elastic turbulence, the cross polymer stress  $\Sigma$  grows much faster than linearly in  $Wi$ , as already shown in Fig. 1. Also the squared polymer elongation in elastic turbulence grows slightly faster than its laminar value and at large  $Wi$  the ratio  $\langle \text{tr } \sigma \rangle / \Sigma$  appears to

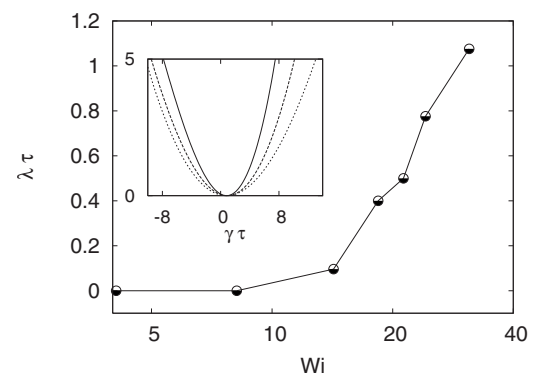


FIG. 4. Lagrangian Lyapunov exponent rescaled with polymer relaxation time  $\tau$  as a function of the Weissenberg number. Inset: Cramer function for three different Weissenberg numbers:  $Wi=18.4$  (solid line),  $Wi=24.2$  (dashed line), and  $Wi=31$  (dotted line).

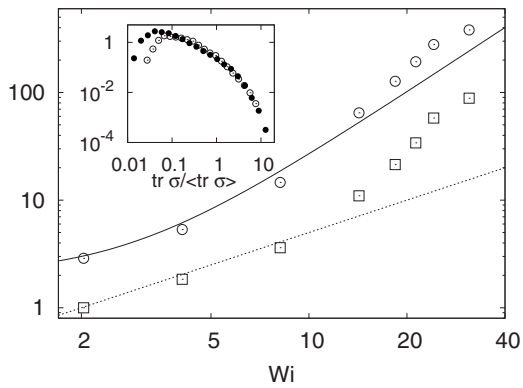


FIG. 5. Average polymer elongation  $\langle tr\sigma \rangle$  (circles) and polymer stress amplitude  $\Sigma$  (squares) as a function of  $Wi$ . Lines represent the laminar behaviors  $2 + Wi^2/4$  (continuous) and  $Wi/2$  (dotted). In the inset, the probability density functions of  $tr\sigma$  for  $Wi=18.4$  (open circles) and  $Wi=31$  (filled circles) are shown.

become constant. The probability density function of  $tr\sigma$  shows elongations up to 15 times the average elongation with a distribution that, for strong elongations, becomes independent of  $Wi$ .

Summarizing, we have shown that elastic turbulence can be successfully reproduced numerically with the aid of a widely known viscoelastic model of polymer solutions (the Oldroyd-B model) and a simple geometrical setup (the two-dimensional Kolmogorov flow). Most observed features have a strong qualitative resemblance with experimental results. Quantitative differences exist, however, and may be traced back to the two-dimensional or to the boundaryless nature of our toy flow, or both. In our opinion, this represents a motivation for focusing our attention on statistical aspects rather than fluid-mechanical ones [26]. The surprising result is precisely that, notwithstanding the blatant differences, most statistical features are very similar. Such findings indeed pave the way for a theoretical understanding of elastic turbulence based on extremely simplified fluid models.

We thank V. Steinberg for valuable discussions. This work was carried out under the auspices of the National Nuclear Security Administration of the U.S. Department of Energy at Los Alamos National Laboratory under Contract No. DE-AC52-06NA25396. S.B. acknowledges the support of TEKES-2007 “Multimodel” project.

- 
- [1] A. Groisman and V. Steinberg, *Nature* **405**, 53 (2000).
  - [2] A. Groisman and V. Steinberg, *Nature* **410**, 905 (2001).
  - [3] T. Burghlea, E. Segre, I. Bar-Joseph, A. Groisman, and V. Steinberg, *Phys. Rev. E* **69**, 066305 (2004).
  - [4] P. E. Arratia, G. A. Voth, and J. P. Gollub, *Phys. Fluids* **17**, 053102 (2005).
  - [5] E. Balkovsky, A. Fouxon, and V. Lebedev, *Phys. Rev. E* **64**, 056301 (2001).
  - [6] A. Fouxon and V. Lebedev, *Phys. Fluids* **15**, 2060 (2003).
  - [7] R. B. Bird, C. F. Curtiss, R. C. Armstrong, and O. Hassager, *Dynamics of Polymeric Fluids* (Wiley, New York, 1987), Vol. 2.
  - [8] V. I. Arnold and L. Meshalkin, *Usp. Mat. Nauk* **15**, 247 (1960).
  - [9] G. Boffetta, A. Celani, A. Mazzino, A. Puliafito, and M. Vergassola, *J. Fluid Mech.* **523**, 161 (2005).
  - [10] L. Meshalkin and Y. G. Sinai, *J. Appl. Math. Mech.* **25**, 1700 (1961).
  - [11] R. G. Larson, *Rheol. Acta* **31**, 213 (1992).
  - [12] A. Groisman and V. Steinberg, *Phys. Rev. Lett.* **77**, 1480 (1996).
  - [13] R. G. Larson, E. S. G. Shaqfeh, and S. J. Muller, *J. Fluid Mech.* **218**, 573 (1990).
  - [14] E. S. G. Shaqfeh, *Annu. Rev. Fluid Mech.* **28**, 129 (1999).
  - [15] A. Groisman and V. Steinberg, *Phys. Fluids* **10**, 2451 (1998).
  - [16] K. Arora, R. Sureshkumar, and B. Khomami, *J. Non-Newtonian Fluid Mech.* **108**, 209 (2002).
  - [17] A. N. Morozov and W. van Saarloos, *Phys. Rep.* **447**, 112 (2007).
  - [18] A. Groisman and V. Steinberg, *New J. Phys.* **6**, 29 (2004).
  - [19] R. Sureshkumar and A. N. Beris, *J. Non-Newtonian Fluid Mech.* **60**, 53 (1995).
  - [20] T. Vaithianathan and L. R. Collins, *J. Comput. Phys.* **187**, 1 (2003).
  - [21] G. Boffetta, A. Celani, and A. Mazzino, *Phys. Rev. E* **71**, 036307 (2005).
  - [22] T. Burghlea, E. Segre, and V. Steinberg, *Phys. Fluids* **19**, 053104 (2007).
  - [23] G. Paladin and A. Vulpiani, *Phys. Rep.* **156**, 147 (1987).
  - [24] G. Boffetta, A. Celani, and S. Musacchio, *Phys. Rev. Lett.* **91**, 034501 (2003).
  - [25] T. Burghlea, E. Segre, and V. Steinberg, *Europhys. Lett.* **68**, 529 (2004).
  - [26] D. G. Thomas, R. Sureshkumar, and B. Khomami, *Phys. Rev. Lett.* **97**, 054501 (2006).